Spatially and Reversibly Actuating Soft Gel Structure by Harnessing Multimode Elastic Instabilities

Yingzhi Liu[1,2§], Ansu Sun[2§], Sreepathy Sridhar[2], Zhenghong Li[1,2], Zhuofan Qin[2], Ji Liu[3], Xue Chen[2], Haibao Lu[1], Ben Zhong Tang[4]* and Ben Bin Xu[2]**

[1]Science and Technology on Advanced Composites in Special Environments Laboratory, Harbin Institute of Technology, Harbin, Heilongjiang, 150080, China.

[2]Smart Materials and Surfaces Laboratory, Faculty of Engineering and Environment, Northumbria University, Newcastle upon Tyne, NE1 8ST, UK.

[3]Department of Mechanical and Energy Engineering, Southern University of Science and Technology, Shenzhen, 518055, China.

[4]Department of Chemistry, The Hong Kong Branch of Chinese National Engineering Research Center for Tissue Restoration and Reconstruction and Institute for Advanced Study, The Hong Kong University of Science and Technology, Clear Water Bay, Kowloon, Hong Kong, China.

*Corresponding Author:

E-mail: luhb@hit.edu.cn (Haibao Lu);

E-mail: tangbenz@ust.hk (Ben Zhong Tang);

E-mail: ben.xu@northumbria.ac.uk (Ben Bin Xu)

[§]Yingzhi Liu and Ansu Sun contributed equally to this work.

KEYWORDS: Hydrogel, swelling, creasing, buckling, shape transformation

ABSTRACT:

Autonomous shape transformation holds the key in developing high-performance soft robotics technology, the search for pronounced actuation mechanisms is an ongoing mission. Here, we present the programmable shape morphing of three-dimensional (3D) curved gel structure by harnessing multimode mechanical instabilities during free swelling. First of all, the coupling of buckling and creasing occur at the dedicated region of gel structure, which are attributed to the edge and surface instabilities resulted from structure-defined spatial nonuniformity of swelling. The subsequent developments of post-buckling morphology and crease pattern collaboratively drive a structural transformation of gel part from the 'open' state to the 'close' state, thus realise the function of gripping. By utilising the multi-stimuli responsive nature of hydrogel, we recover the swollen gel structure to its initial state, enabling reproducible and cyclic shape evolution. The described soft gel structure capable of shape transformation brings a variety of advantages such as easy to fabricate, large strain transformation, efficient actuation and high strength-to-weight ratio, which is anticipated to provide guidance for future applications in soft robotics, flexible electronics and off-shore engineering and healthcare products.

1. INTRODUCTION

Soft matter based bio-system widely exist in nature to support lives such as octopus, starfish, caterpillars, etc., by fulfilling adaptive shape changes and responsive motions to allow them to survive in the complex environments[1-5]. Inspired by those features, a number of soft actuator concepts[6-11] have been developed to mimic dedicated actuations/motions, e.g., soft grippers actuated by inflation of a pneumatic network to manipulate fragile and irregular objects[12]; a humidity and light driven liquid-crystal-network actuator[13] to mimic self-shape-morphing of flowers; bellows-like actuators[14] with origami structure enabled various motions. The discovery of superior bio-inspired robotic structure/mechanism with desired working capacity, efficient actuation, high strength-to-weight ratio, on demand shape programmability and low cost, is highly desired for frontier engineering applications.

Responsive hydrogel based configurable structures can undergo shape transformation and perform complicated pattern generation spontaneously and reversibly at the presence of external stimulus, such as temperature, ionic strength, pH, light, solvent, and electric field[15-19]. Together with its soft, biodegradable and biocompatible properties, hydrogel has been seen as an ideal candidate to build soft robotics[20], soft actuators[21-22] and soft electronics[23-24]. Notably, Palleau et al.[25] created soft hydrogel tweezers through electrically assisted ionoprinting, and demonstrated the gripping/releasing of small objects. By using 3D printing technique, Xu and co-workers[26] fabricated an airplane-like swimming gel robot that could remotely control the different motions under near-infrared light. Yuk et al.[20] exploited hydraulic actuation of hydrogels to develop soft

robotics which capable of optical and sonic camouflage in water. While above attempts provide advancements in exploring novel actuating mechanism, the overall fabrication, assembly and actuation of those devices heavily relay on the supports from instrument and infrastructure, which will considerably limit the application/commercialisation of hydrogel actuators at scale-up level.

Mechanical instabilities including wrinkling[27-33], creasing[34-37], folding[38-40], ridging[41-44], buckling[45-46] and bending[47] have brought unique approach to realise programmable shape transformations of soft tissue. When the hydrogel is under isotropic swelling, it cannot cause instability to induce structural deformation, only a uniform increase in volume is induced (**Figure 1a**). Therefore, substantial efforts have been devoted in developing planar structure with multi-layer[48-49], different responsiveness[50] or density gradient[51-52] to improve the controllability and efficiency of instability-induced 3D shape transformations, or preparing homogeneous hydrogel structures upon constrained swelling[53] (**Figure 1a-b**). Especially, Gong et al. studied the formation of surface creasing and bulk bending of a piece of hydrogel with cuboid shape or disc-shape induced by free swelling[54-55]. Recently, researchers explore the generation of instabilities on the curved structures[53, 56], where the structural anisotropy guided formation of non-uniform stresses could create instabilities in a designable and efficient fashion to induce the shape transformations, as being discussed by non-Euclidean shell theory[57-58]. However, the actuation of shape transformation by modulating and coordinating multimode instabilities induced by free swelling in a 3D curved gel structure have been rarely exploited.

In this work, we propose a novel actuation technology by introducing locally confined

development of mechanical instabilities on a 3D curved gel structure with the shape of 'semi-cylinder shell'. Under freestanding swelling, instabilities are firstly initialised at dedicated areas with the buckling occurring on the axial edges and the creasing on the circumferential outer surface. Subsequently, the developments of post-buckling geometries and crease patterns enable a directional releasing of strain energy, thus drive the shape transformation of gel structure from 'open' state to the 'close' state, and realise the function of gripping. By optimising the inputs from the gel composition and geometrical design, we achieve swelling-driven programmable shape morphing and demonstrate the potential application as an autonomous gripper.

2. RESULTS AND DISCUSSION

The 3D curved gel structure with the shape of 'semi-cylinder shell' is designed and fabricated by synthesising the poly(acrylamide-co-sodium acrylate) hydrogel (PAAm-*co*-NaAc) in a 3D printed mould, as shown in **Figure 1c** (more details in *experimental section*). The preliminary thought to take the curved shell design is to utilize the stain growth on circumferential direction to achieve a 'close' state (see **Figure S1**). The obtained hydrogel structure is subsequently immersed into deionized (DI) water to introduce freestanding swelling. An exemplified design is selected to show the swelling-induced morphological developments, with outer diameter D_{out}=10 mm, inner diameter D_{in}=5 mm, initial thickness $H_0 = (D_{out} - D_{in})/2$=2.5 mm, initial axial length L_0=10 mm and open angle θ=180°. After swelling, morphological developments

are observed on the specific locations: buckling (**Figure 1d-e**) occurring at the axial edges and reticulated creases (**Figure 1f-g**) appearing on the circumferential outer surface. The geometrical characteristic of this designed structure enabled co-existence of buckling and creasing with clear preferences on location, unveils an interesting energy distribution throughout the designed gel structure, which has not been reported elsewhere.

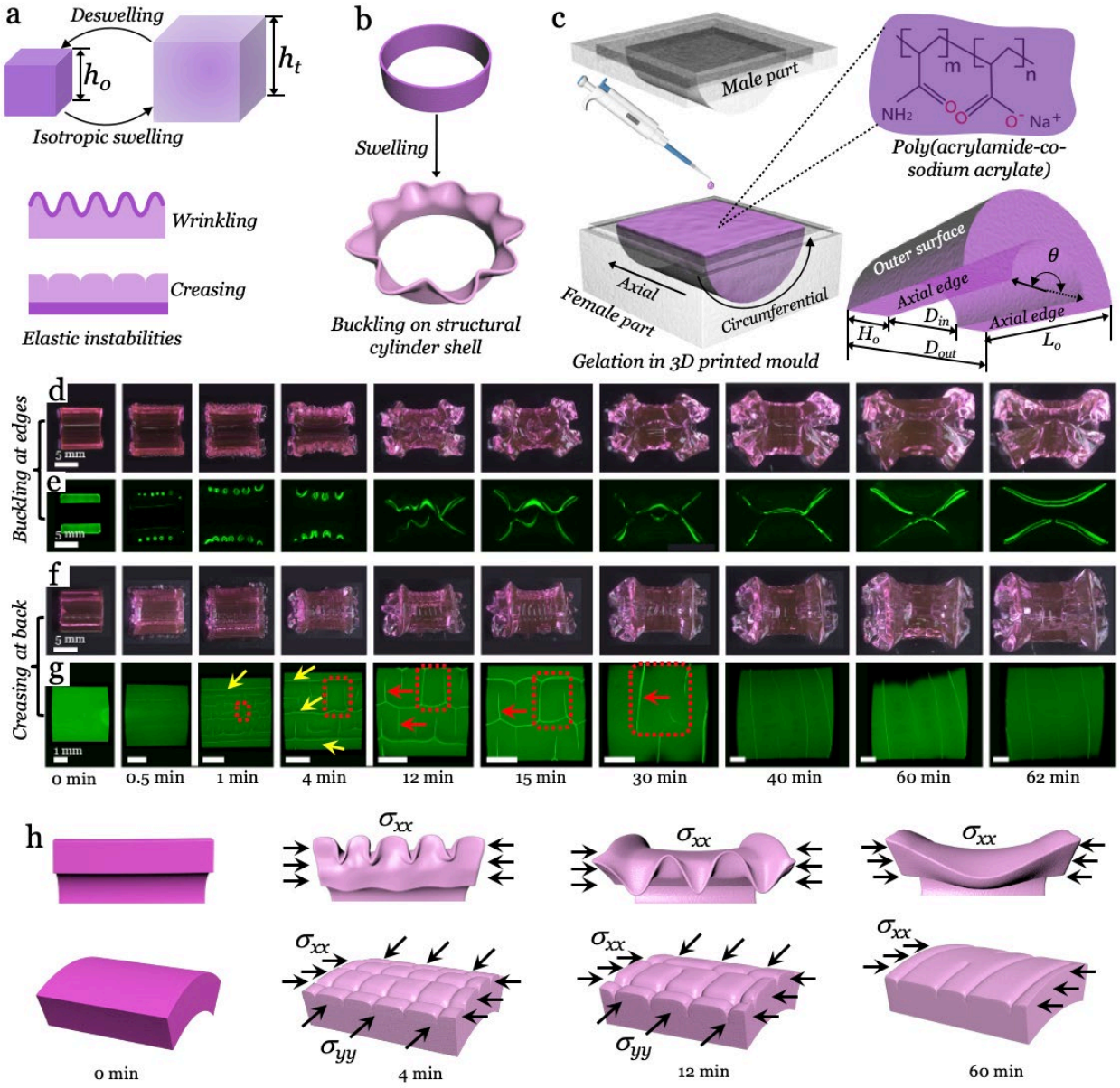

Figure 1. Swelling-induced multimode elastic instabilities. a) Illustration of the isotropic swelling of a homogeneous gel unit and the swelling induced instabilities in a multi-layer gel structure. b) The schematic of buckling on the edge of a gel cylinder shell. c) Schematic illustration of fabricating gel structure by injecting the pre-solution into a 3D printed 'semi-cylinder shell' mould, the molecular structure of hydrogel, and the definitions of geometrical factors. The observations of morphologies at various time intervals on the axial edges of the gel structure under d) optical microscope and e) Laser Scanning Confocal Fluorescence Microscope (LSCM); and on circumferential outer surface with f) optical microscope and g) LSCM on the selective zone in optical image (scale bar = 1 mm). h) the illustration of stress states for the edge and back areas at designated time. Images (d-f) are formatted with the same scale bar of 5 mm.

The buckling at the axial edges shows an early onset (< 30 seconds, **Figure 1d**), then a post-buckling development is observed with a reduction in buckling numbers but an increase in wavelength (λ, **Figure 1e**). Another interesting event taking place at the circumferential outer surface is the initiation of axial creasing lines, whose length aligns with the axial direction at round 30 seconds (**Figure 1g**), which means that the region undergoes circumferential compression. The overall stress evolutions as per location are illustrated in **Figure 1h** with uniaxial stress localizing (σ_{xx}) on the edge section. However, a translational biaxial stress state (σ_{xx} and σ_{yy}, σ_{yy} represent the stress in circumferential direction) is presented for back area where an equi-biaxial stress state ($\sigma_{xx}=\sigma_{yy}$) appears to occur soon as the hydrogel swells, by generating a biaxial 'grid' type creasing at around 1 min and such biaxial creasing explicitly grows till 12 mins with the aspect ratio of a single unit of 'grid' (see red dash box in **Figure 1g**) being reasonably maintained. When the gel structure swells from 12 mins to 30 mins, the neighbouring axial creasing separates from each other faster than the circumferential creases, leading to the vanish of axial creasing lines at 30 mins (see red and yellow arrows in **Figure 1g**). The circumferential creases rule the place thereafter, till

reaching the global isotropic swelling state (see **Figure S2**) after 4 hours. The trans-directional development of creasing pattern from axial creasing lines to biaxial 'grid', then to circumferential creases, represent a self-regulation of strain energy and then a release of the strain energy in circumferential direction.

Macroscopically, we observe a global transformation of the gel structure from 'open' to 'close', then returning to the 'open' state (**Figure 1d-1e**). The post-buckling development and evolution of creasing pattern collaboratively drive the gel structure to close from 4 mins to 15 mins. The geometrical developments at the axial edges make a direct effort to allow the edges to physically contact with each other; on the other hand, the release of energy in circumferential direction regulated by the creasing pattern support these buckling developments to accelerate structure closing. Beyond that, an adaptive structural harmonization starts from 30 mins, by developing a single buckling pattern at each axial edge towards $\lambda > L$ (L refers to the axial length after gel structure swollen). The gel structure stays at the 'close' configuration until 60 mins, then gradually reopens. Once reaching the end of morphing process, all surfaces of the gel structure resume to smooth state with the instabilities patterns completely disappeared (**Figure S2**). An isotropic swollen 'semi-cylindrical shell' shaped gel structure is presented (D_{out}=29.2 mm, H=7.2 mm and L=28 mm).

Once the gel structure swells, water molecules diffuse into the surface to create a thin gradient layer with swelling induced strain, therefore leading to a multi-layer configuration in a finite depth with generating a spatially non-uniform stress in the thin gradient layer. Wavy

buckling patterns are found on both of the axial edges (**Figure 2a**) and the circumferential edges (**Figure S3**). However, the post-buckling phenomenon on the axial edges with strong out of plane morphological development directly contribute to the 'closing' of gel structure. The crease patterns are observed both on the circumferential inner (**Figure S3**) and outer (**Figure 2b**) surfaces initially, but the full sequence transition (from axial creasing lines to biaxial creasing 'grid', then to circumferential creasing lines) only occurs at the circumferential outer surface, where the trans-directional regulation on strain energy leads to a releasing of strain energy along the circumferential direction and effectively drive the shape morphing. It is worth noting that hydrogel parts in 'hemi-spherical shell' shape are also fabricated, and the observations of morphologies at various time intervals of the hydrogel part are summarised in **Figure S4**, where a similar shape transformation from 'open' to 'close' is found by swelling the part. However, the underlying mechanics seems much more complicated as the strain development on the hemi-spherical shell is arbitrary. Therefore, we defer the research of this structure in the future work.

To trace the morphological evolutions, we plot the wavelength (λ) and amplitude (A) of the buckling in **Figure 2c**, and creases spacing and depth (χ, μ) in **Figure 2d** as the function of swelling time (t). When swelling progresses, the coalescence of adjacent buckling is observed. When the gel structure transforms from 'open' state (green area) into 'close' state (pink area), the wavelength keeps growing, while the amplitude increases to the peak value at the closure and then decreases to 0 (**Figure 2c**). In **Figure 2d**, the creases depths (μ_H and μ_V) first achieve maximum and then start to fade. evolution trend of average crease spacing (χ_H and χ_V) follows a linear relationship

with the square root of swelling time, which agrees well with the theory[59-60].

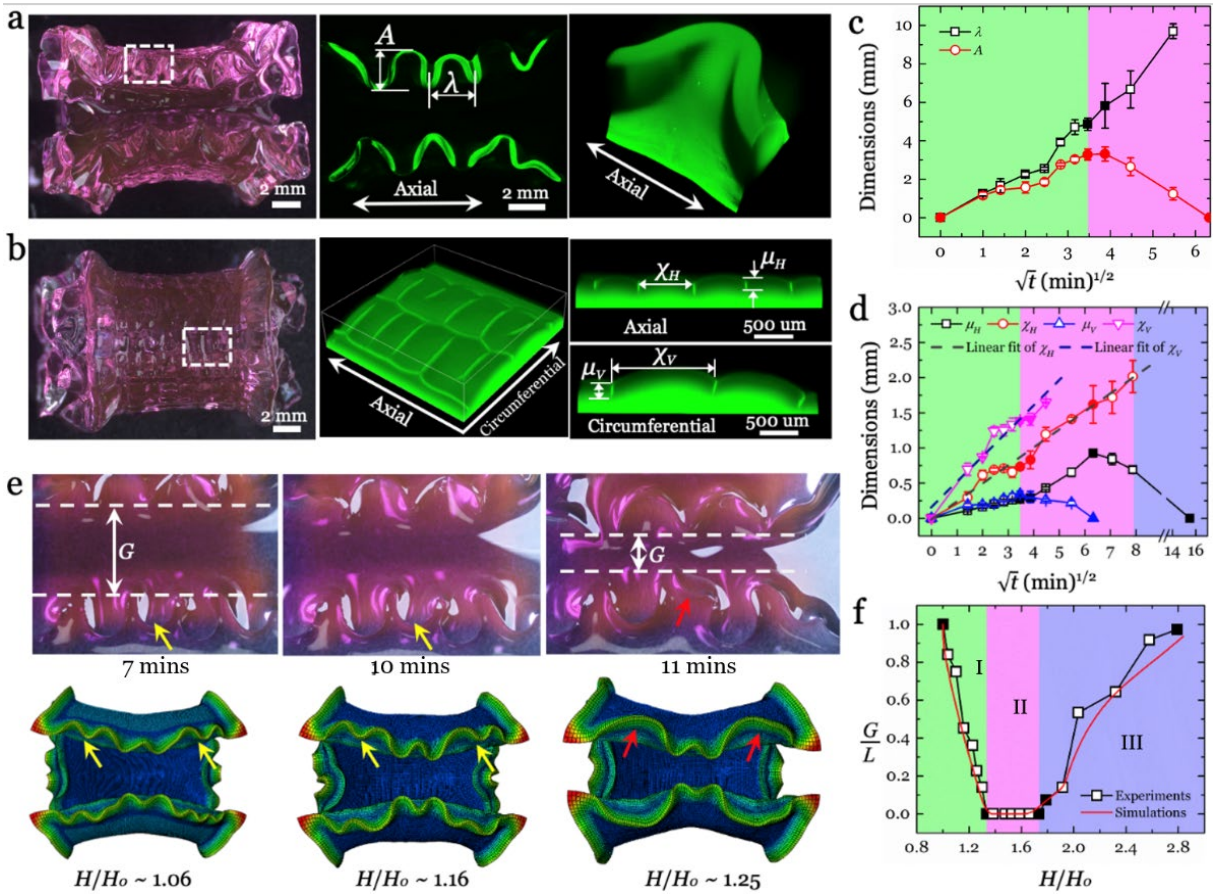

Figure 2. Geometrical analysis on the multimode instabilities and their collaborative effect on the transformation of gel structure. The observations of swelling-induced morphological developments at 8 mins for the axial edges with a) optical microscope, fluorescence microscope and reconstructed 3D image from LCSM based on the selected area in optical image, and for the circumferential out surface with b) optical microscope, LCSM and the cross-sections along the axial and circumferential direction from LSCM based on the selected area in optical image. The analytical plots of time dependent evolutions of structure deformation during swelling: c) wavelength (λ) and amplitude (A) of buckling, d) surface crease depths (μ_H and μ_V) and crease spacings (χ_H and χ_V). e) The experimental observation and finite element simulation of the post-buckling development. f) G/L versus H/H_0. Green area: I-closing regime; pink area: II-holding regime; purple area: III-reopening regime.

We next investigate how buckling contribute to the global 'closure' of soft structure. The

degree of swelling is defined as H/H_0, where H is the thickness of swollen structure at certain swelling time. The development of wavy buckling profile on the axial edges can be evidenced with merging neighbouring waves into a big one (see the yellow and red arrows in **Figure 2e** and **Movies S1**). A diagram (**Figure 2f**) is created by plotting the normalized closing factor of G/L, where G refers to the gap distance between edges (see **Figure 2e**). **Figure 2f** presents three regimes for the morphing of gel structure: I-closing regime with G/L decreasing from 1 to 0 and close at G/L=0 (green area), the swelling time when G/L=0 is defined as the close time; II-holding regime with G/L remaining at 0 (pink area); III-reopening regime with G/L gradually increasing from 0 to ~1 (purple area), the open time is the time when G/L starts increasing from 0, and the recovery time is the time when G/L returns to ~1. The results of finite element analysis (full simulation in **Movies S2**, **Figure 2e-f**) show a good agreement with the experiment results.

We then explore the efficiency of shape transformation by tuning the geometrical variables with different initial thicknesses (H_0) in **Figure 3a**, initial axial lengths (L_0) in **Figure 3b** and open angles (θ) in **Figure 3c**. In **Figure 3a**, we fix the values of outer diameter (D_{out}=10 mm), angle (θ=180°) and length (L_0=10 mm), thus, the area of circumferential outer surface ($S_{cy} = \pi D_{out} L_0 \theta / 360°$) remains unchanged, while the area of annulus surface area ($S_{an} = 0.25\pi\left(D_{out}^2 - D_{in}^2\right)\theta / 360°$) increases with the increases of thickness. It is found that the gel structure with a smaller H_0 reaches the full closure earlier. The gel structure with H_0= 5 mm (D_{in} = 0) cannot close completely, because the bending stiffness resist the closing. In **Figure 3b**, S_{an} remains unchanged while S_{cy} decreases as L_0 decreases when the values of outer diameter (D_{out}=10

mm), angle (θ=180°) and thickness (H_0=2.5 mm) keep constant. We discover that the gel structure with longer axial length is likely to hold the 'closing' stage for an extended period. The gel structure with L_0 of 3 mm does not close completely, and the reason could be the insufficient axial length which does not allow the buckling profile to evolve. In **Figure 3c**, without changing D_{out}, L_0 and H_0 (D_{out}= L_0=10 mm, H_0=2.5 mm), both S_{an} and S_{cy} increase as θ increases. The gel structure with bigger θ need less time to close, and those with smaller θ (e.g. 120° and 150°) are unable to reach a full closure. With the decrease of θ, extra circumferential distance is needed for gel structure to reach the 'close' state, which bring more challenges to fulfil this configuration change.

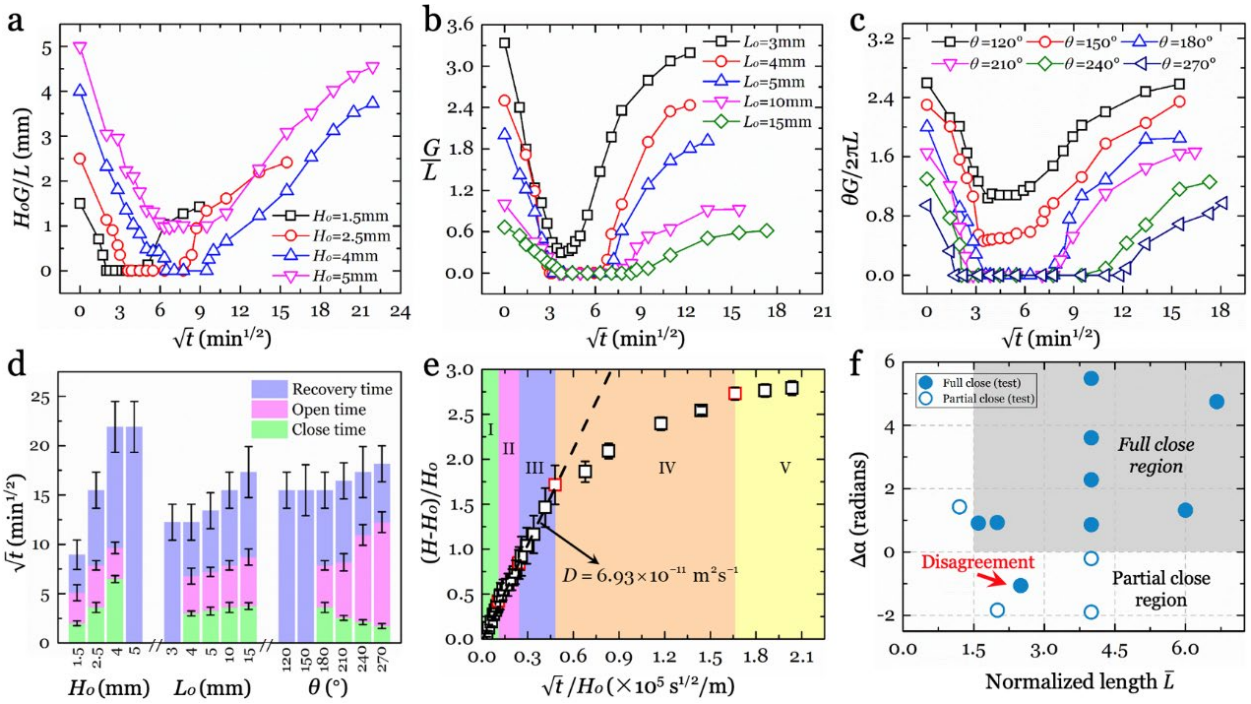

Figure 3. Time dependent shape morphing analysis by varying geometrical factors. a) Different initial thicknesses (H_0), D_{out}=L_0=10 mm, θ=180°. b) Different initial Lengths (L_0), D_{out}=10 mm, H_0=2.5 mm, θ=180°. c) Different initial angles (θ), D_{out}= L_0=10 mm, H_0=2.5 mm. d) The effects of geometry factors on shape transformation times. e) The normalized thickness follows an apparently diffusive scaling at short times (slope of the dashed line). f) Phase diagram by plotting the bending angle difference $\Delta\alpha$ and normalized length $\bar{L}$, shaded area represents the full close region (i.e. G/L = 0) and un-shaded part is the partial close region (i.e. G/L > 0).

Apparently, the 'close' state is easier to be achieved for the gel structure with a larger S_{cy} and a smaller S_{an}, where the geometrical landscape is energetically favoured by the post-buckling development. Longer open time and recovery time are needed once the volume of gel structure increases, i.e. thickness/length/angle increased (see **Figure 3d**), providing a better control to morph structure. In **Figure 3e**, we map the swelling kinetics by plotting the change in thickness of the gel structure normalized by its initial thickness, $(H-H_0)/H_0$ as a function of $\sqrt{t}/H_0$. After transforming from 'open' state into 'close' state (regime I, green area), and then 'holding' stage (regime II, pink area), the gel structure recovers (regime III, purple area) to the 'semi-cylindrical shell' shape and regain the homogeneity. Even at this time, the gel structure is not fully swollen, and it continues swelling isotropically (regime IV, orange area) to the final state (regime V, yellow area) in which the hydrogel could no longer absorb the water. By linear fitting of the initial slope of data in **Figure 3e**, a diffusion coefficient constant of D=6.93×10^{-11} m^{2}s^{-1} is estimated from the 'open' state to the end of 'holding' stage, which is in the similar magnitude to that for polyacrylamide hydrogel in previous reports[16, 61-62].

We next numerically scale the 'close' state by utilising Euler-Bernoulli curved-beam theory and considering the swelling competition between the circumferential outer surface and annulus surfaces (see *experimental section* for the details). We define $\Delta\alpha > 0$ and $\overline{L} > \overline{L}_c$ with the bending angle difference $\Delta\alpha = ac\left(H/H_0 - 1\right)\theta' - \left(2\pi - \theta'\right)$ and the normalized length $\overline{L} = L_0/H_0$, where a is the parameter associated with the geometric parameters of the sample and $a = D_{out}\ln\left(D_{out}/D_{in}\right)/\left(D_{out}\ln\left(D_{out}/D_{in}\right) - 2H_0\right)$, $\theta' = \pi\theta/360°$, and H/H_0 is the swelling ratio after

regime III, at which the gel structure starts to isotropic swell. The two parameters c and $\bar{L}_c$ generally depend on the diffusion kinetics and the mechanical behaviour of the hydrogel. Currently, there is no explicit mathematical expression to calculate the exact values of them. Here we estimate the two parameter values by our experiments, i.e., choosing the values which can satisfy the most experimental data. Therefore, c = 0.19 and $\bar{L}_c$ =1.5 are taken for the best fit of the current experiments. A phase diagram (in terms of $\Delta\alpha$ and $\bar{L}$, **Figure 3f**) can be therefore created to show the threshold of closure by applying above definitions and experimental inputs. Overall, a good quantitative agreement has been reached between theoretical predictions and experimental results, with one exceptional data (pointed out by red arrow in **Figure 3f**) from a gel structure with a bigger thickness (H_0= 4 mm). Since Euler-Bernoulli theory is only applicable to thin beams, its estimation on the shift of bending angle for a thick gel structure might be less accurate, which we decide to extend the research on modelling the shape morphing in the thick structure in the future work.

The swelling behaviour of the gel structure (D_{out}= L_0=10 mm, D_{in}=5 mm, θ=180°) is assessed with different BisAA contents in **Figure S5a**. For the gel structures with higher BisAA concentrations (e.g. 37.4 mM and 44.2 mM in **Figure S5a**), they are hardly to reach a full closure. For those gel structures with lower BisAA concentrations (e.g. between 3.4 mM and 13.6 mM in **Figure S5c**), their close time are almost identical, while the automatic open time and the full recovery time decrease as BisAA content increases. The swelling behaviour of gel structure is also studied for swelling at various concentrations of phosphate buffer saline solution (PBS). Our hydrogel has an ionic strength of 168 mM, which is similar to the ionic strength in 0.01 M PBS

(156.6 mM), thus the gel structure achieves limited swelling when immerse it into 0.01 M PBS (**Figure S5d**). As shown in **Figure S5b**, with the lower concentration of PBS, the gel structure close more rapidly. While these results show some interesting phenomena, we unfortunately have not got systematic clue from these results. We will keep exploring this part of research in our future work plan to create complicated swelling gradients in the soft gel structure.

We perform the cyclic actuation (**Figure 4a**) by de-swelling the 're-opened' gel structure through a conventional air-drying process, then saturating in 0.01 M PBS for 10 mins till reaching to the original shape, from which a new swelling cycle starts (**Figure S6**). Afterwards, we assess the reproducibility of shape morphing of gel structure with D_{out}=L_0=10 mm, D_{in}=5 mm, θ=180°. The gel structure presents a good reproducibility for 30 cycles (**Figure 4b**). After 30 cycles, the sample cannot recover completely, which could be attributed to trivial structure degeneration (fatigue) during the experiments. We further design gel grippers with four fingers to demonstrate their efficiencies of autonomous gripping. Both hydrogel grippers can be actuated in DI water within 3 mins to reach full closure and 20 mins to fully reopen in DI water, as shown in **Figure 4c-d**. These four-finger designs optimise the shape morphing by dramatically reducing the closing time. There are no significant differences on actuation performance for the devices between the designs of sharp finger and flat finger. A demonstration of weight lifting is conducted for the gripper (with about 0.14 g weight), by using it to pick up a small magnetic stirrer (weight is about 2 g) from the water (**Figure 4e** and **Movie S3**), which is 15 folds of the weight of gripper. This gripping strength could be potentially applied in the soft robotics for off-shore/marine engineering.

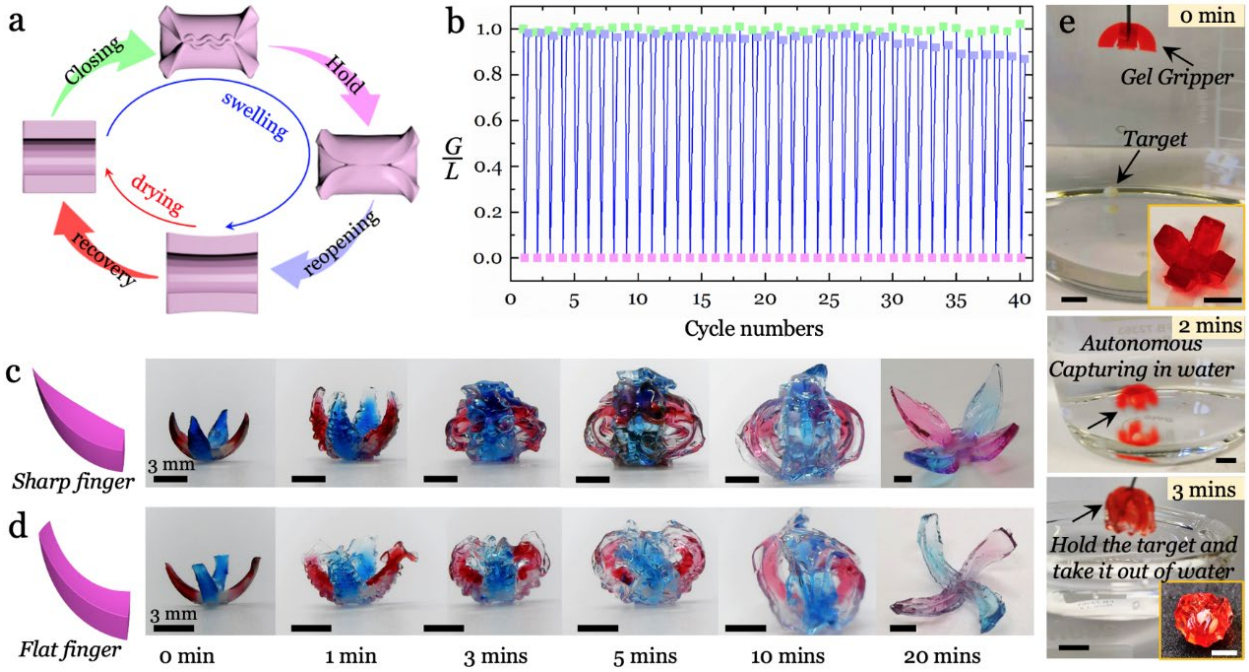

Figure 4. The reproducibility and demonstration of hydrogel structure. a) Schematic illustration of a loop of open-close-recovery cycle, and b) cyclic testing with open-close for gel structure. Time lapsed gripping motion captures for the hydrogel gripper with c) sharp finger design and d) flat finger design. e) A demonstration of gripping strength by using the designed hydrogel gripper (4 fingers, D_{out}=10 mm, D_{in}=5 mm, L_0=3 mm, θ=180°) to pick up a magnetic stirrer from the water, the scale bar is 5 mm.

3. CONCLUSIONS

We describe an autonomous shape transformation of 3D curved gel structure by harnessing swelling-induced multimode mechanical instabilities. The initiation and programmable developments of multimode instabilities including buckling at axial edges and creasing at circumferential outer surface have been realised in the dedicated regions. The co-existence and the regional developments of buckling and creases collaboratively drive the global shape morphing of the gel structure from the 'open' state to the 'close' state. Numerical analysis creates a phase

diagram to understand the effects of the geometries and swelling ratio on the 'gripping' efficiency. We successfully demonstrate the actuations of several conceptual designs with good reproducibility by tailoring the structure and tuning the swelling. This mechanics enabled shape transformation of 3D curved gel structure bring a valuable approach to design and develop soft robotics with desired efficiency and integrability, which can be applied in future healthcare device, human-machine interface, wearable electronics, etc.

4. EXPERIMENTAL SECTION

3D printing mould: To fabricate 3D curved gel structure with the shape of 'semi-cylindrical shell', moulds were created *via* Strasys® Objet 24 3D printing system (Z Resolution: 28 μm). The moulds were designed in Solidworks software before printing. The printed parts were cleaned and rinsed with isopropanol (IPA), before being annealed on a hot plate at 100 °C for 15 mins to allow the printed parts to be fully matured. The assembly of gelation chamber was constructed by the printed male and female parts and wax based sealants to prevent any possible leaking.

Synthesis of hydrogels: The polyacrylamide hydrogel was synthesized by free-radical polymerization using ammonium persulfate as initiator. 1 mL aqueous pre-gel solution containing 1173.3 mM acrylamide (monomer), 168.6 mM sodium acrylate (NaAc, charged monomer) and 6.8 mM N,N′-methylenebisacrylamide (BisAA, crosslinker) were prepared, and degassed under 1 mTorr for 10 mins after mixing and dissolving sufficiently. After that, this pre-gel solution which

mixed with 1.5 μL of *N,N,N′,N′*-tetramethylethylenediamine (TEMED, accelerator) and 5 μL of a 10 wt% aqueous ammonium persulfate solution (APS) was rapidly loaded into the 3D printing mould. The mould had been treated by 1H,1H,2H,2H-perfluorooctyltrichlorosilane from the vapour-phase at room temperature (23 °C) for 2 hours to facilitate the release of hydrogel structure after 30 mins gelation process. All chemicals were used as received from Sigma Aldrich.

Characterization: To monitor the formation and evolution of surface/structure morphologies, a trace amount of Rhodamine-B monomer was added into the pre-gel solution to enhance the visual contrast and allow the high resolution imaging with a camera. The as-fabricated hydrogel was submerged into DI water to swell. During the swelling process, the hydrogel was gently taken out from DI water to observe under optical microscope (Nikon LV100) at regular time intervals. A small amount of fluorescein isothiocyanate-dextran (~1 mg) was added into the pre-gel mixture to label the gel structure and facilitate imaging under LSCM (Nikon A1R).

Finite element simulations: Finite element simulations were conducted using the commercial software (ABAQUS). The gel was modelled as an incompressible Neo-Hookean material. Based on the analogy between heat transfer and solvent diffusion, thermal expansion was used here to simulate swelling, the corresponding coupled temperature-displacement analysis was conducted. It is noted that the simulations focused on the global structure deformations while the local surface creases caused by surface instability were neglected considering the numerical convergence. The explicit dynamic solver was used in the simulations, and the static results were obtained after the

kinetic energy was dissipated.

Numerical approach for fully-closed state: The 'semi-cylindrical shell' shaped gel structure could be regarded as an initially curved beam with the cross-section of $L_0 \times H_0$. $\theta' = \pi\theta/360°$ is introduced for convenient. By Euler-Bernoulli beam theory and scaling analysis, the bending angle of the beam due to the tension at the outer surface could be roughly estimated as:

$$\alpha = a\varepsilon_0\theta' \tag{1}$$

Where $a = D_{out}\ln\left(D_{out}/D_{in}\right)\Big/\left(D_{out}\ln\left(D_{out}/D_{in}\right) - 2H_0\right)$, ε_0 is the tensile strain on the outer surface, and ε_0 is related to the swelling strain (H/H_0-1), with H/H_0 being the swelling ratio for the gel structure swelling after regime III, at which the gel structure started to swell homogeneously. The explicit expression of ε_0 as a function of (H/H_0-1) depends on the diffusion kinetics and the mechanical behaviour of the hydrogel. Here for simplicity, we take $\varepsilon_0 = c(H/H_0-1)$, with c being a constant parameter. Then **Equation (1)** could be rewritten as:

$$\alpha = ac\left(H/H_0 - 1\right)\theta' \tag{2}$$

To reach the fully-closed state, the gel structure must bend/rotate a minimum angle of ($2\pi-\theta'$). Then combining **Equation (2)**, we obtain the following requirement on the bending angle:

$$\Delta\alpha > 0 \tag{3}$$

with $\Delta\alpha = ac\left(H/H_0 - 1\right)\theta' - \left(2\pi - \theta'\right)$.

We also need consider the swelling competition between the circumferential outer surface and annulus surfaces. If the fabricated gel structure was too short (i.e. small length), the water molecules would quickly enter through the annulus surfaces and mainly diffuse along the gel

length. In this case, the inner-core beneath the circumferential outer surface would be in the partially swollen state, and the tension induced by the swelling mismatch between the circumferential outer surface and inner core would not be large enough to induce bending. To assess this effect, the following requirement on the structure length is proposed:

$$\bar{L} > \bar{L}_c \tag{4}$$

with normalized length $\bar{L} = L_0 / H_0$. $\bar{L}_c$ is the critical normalized length for full closure. By combining **Equation (3)** and **(4)**, we establish the criterion for the appearance of full closure state, based on the geometries and swelling of gel structure.

ASSOCIATED CONTENT

Supporting Information

The Supporting Information in PDF is available free of charge, in addition, we provide the following supporting information in multimedia files:

Supplementary Movie 1: The development of wavy buckling profile on the axial edges by optical microscope (MP4).

Supplementary Movie 2: The finite element analysis results (MP4).

Supplementary Movie 3: A demonstration of gripping strength by using a designed hydrogel gripper to pick up a magnetic stirrer from the water (MP4).

AUTHOR INFORMATION

Corresponding Authors

Haibao Lu − *Science and Technology on Advanced Composites in Special Environments Laboratory, Harbin Institute of Technology, Harbin, Heilongjiang, 150080, China;* E-mail: luhb@hit.edu.cn

Ben Zhong Tang − *Department of Chemistry, The Hong Kong Branch of Chinese National Engineering Research Center for Tissue Restoration and Reconstruction and Institute for Advanced Study, The Hong Kong University of Science and Technology, Clear Water Bay, Kowloon, Hong Kong, China;* E-mail: tangbenz@ust.hk

Ben Bin Xu − *Smart Materials and Surfaces Laboratory, Faculty of Engineering and Environment, Northumbria University, Newcastle upon Tyne, NE1 8ST, UK;* E-mail: ben.xu@northumbria.ac.uk

Authors

Yingzhi Liu − *Science and Technology on Advanced Composites in Special Environments Laboratory, Harbin Institute of Technology, Harbin, Heilongjiang, 150080, China; Smart Materials and Surfaces Laboratory, Faculty of Engineering and Environment, Northumbria University, Newcastle upon Tyne, NE1 8ST, UK*

Ansu Sun − *Smart Materials and Surfaces Laboratory, Faculty of Engineering and Environment, Northumbria University, Newcastle upon Tyne, NE1 8ST, UK*

Sreepathy Sridhar − *Smart Materials and Surfaces Laboratory, Faculty of Engineering and*

Environment, Northumbria University, Newcastle upon Tyne, NE1 8ST, UK

Zhenghong Li − *Science and Technology on Advanced Composites in Special Environments Laboratory, Harbin Institute of Technology, Harbin, Heilongjiang, 150080, China; Smart Materials and Surfaces Laboratory, Faculty of Engineering and Environment, Northumbria University, Newcastle upon Tyne, NE1 8ST, UK*

Zhuofan Qin − *Smart Materials and Surfaces Laboratory, Faculty of Engineering and Environment, Northumbria University, Newcastle upon Tyne, NE1 8ST, UK*

Ji Liu − *Department of Mechanical and Energy Engineering, Southern University of Science and Technology, Shenzhen, 518055, China*

Xue Chen − *Smart Materials and Surfaces Laboratory, Faculty of Engineering and Environment, Northumbria University, Newcastle upon Tyne, NE1 8ST, UK*

Author Contributions

Y.L. and A.S. contributed equally to this work. The idea was initially generated between B.X. and H.L. who piloted the research program and designed the experiments with Y.L. and A.S.. Y.L. and A.S. carried out the experiments with the assistances from S.S. and Z.L. on gel fabrication, 3D printing and pattern transformation. B.X., X.C. and Z.Q. developed the analytical simulations. B.X., Y.L., H.L., J.L. and B.Z.T. analyzed and interpreted the data. B.X., Y.L., H.L., J.L. and B.Z.T. defined the scope together and wrote the paper with contributions from all authors.

Notes

The authors declare no competing interests.

ACKNOWLEDGMENTS

The work was supported by National Natural Science Foundation of China (NSFC) under Grant No. 11672342 and 11725208 and the Engineering and Physical Sciences Research Council (EPSRC) grant-EP/N007921 and Royal Society Kan Tong Po International Fellowship 2019-KTP\R1\191012.

REFERENCES

(1) Wehner, M.; Truby, R. L.; Fitzgerald, D. J.; Mosadegh, B.; Whitesides, G. M.; Lewis, J. A.; Wood, R. J. An Integrated Design and Fabrication Strategy for Entirely Soft, Autonomous Robots. *Nature* **2016,** *536* (7617), 451-455.

(2) Woodward, M. A.; Sitti, M. Morphological Intelligence Counters Foot Slipping in the Desert Locust and Dynamic Robots. *P. Natl. Acad. Sci. USA* **2018,** *115* (36), E8358-E8367.

(3) Elphick, M. R.; Melarange, R. Neural Control of Muscle Relaxation in Echinoderms. *J. Exp. Biol.* **2001,** *204* (5), 875-885.

(4) Lin, H. T.; Leisk, G. G.; Trimmer, B. Goqbot: A Caterpillar-Inspired Soft-Bodied Rolling Robot. *Bioinspir. Biomim.* **2011,** *6* (2), 026007.

(5) Ren, Z.; Hu, W.; Dong, X.; Sitti, M. Multi-Functional Soft-Bodied Jellyfish-Like Swimming. *Nat. Commun.* **2019,** *10* (1), 2703.

(6) Liu, J.; Gao, Y.; Wang, H.; Poling-Skutvik, R.; Osuji, C. O.; Yang, S. Shaping and Locomotion of Soft Robots Using Filament Actuators Made from Liquid Crystal Elastomer–Carbon Nanotube Composites. *Adv. Intell. Syst.* **2020,** *2* (6), 1900163.

(7) Pena-Francesch, A.; Jung, H.; Demirel, M. C.; Sitti, M. Biosynthetic Self-Healing Materials for Soft Machines. *Nat. Mater.* **2020,** *19* (11), 1230-1235.

(8) Dong, X.; Lum, G. Z.; Hu, W.; Zhang, R.; Ren, Z.; Onck, P. R.; Sitti, M. Bioinspired Cilia Arrays with Programmable Nonreciprocal Motion and Metachronal Coordination. *Sci. Adv.* **2020,** *6* (45), eabc9323.

(9) Liu, L.; Broer, D. J.; Onck, P. R. Travelling Waves on Photo-Switchable Patterned Liquid Crystal Polymer Films Directed by Rotating Polarized Light. *Soft Matter* **2019,** *15* (40), 8040-8050.

(10) Matsuda, T.; Kawakami, R.; Namba, R.; Nakajima, T.; Gong, J. P. Mechanoresponsive Self-Growing Hydrogels Inspired by Muscle Training. *Science* **2019,** *363* (6426), 504-508.

(11) Ni, C. J.; Chen, D.; Zhang, Y.; Xie, T.; Zhao, Q. Autonomous Shapeshifting Hydrogels via Temporal Programming of Photoswitchable Dynamic Network. *Chem. Mater.* **2021,** *33* (6), 2046-2053.

(12) Yang, D.; Mosadegh, B.; Ainla, A.; Lee, B.; Khashai, F.; Suo, Z.; Bertoldi, K.; Whitesides, G. M. Buckling of Elastomeric Beams Enables Actuation of Soft Machines. *Adv. Mater.* **2015,** *27* (41), 6323-6327.

(13) Wani, O. M.; Verpaalen, R.; Zeng, H.; Priimagi, A.; Schenning, A. An Artificial Nocturnal Flower via Humidity-Gated Photoactuation in Liquid Crystal Networks. *Adv. Mater.* **2019,** *31* (2), 1805985.

(14) Martinez, R. V.; Fish, C. R.; Chen, X.; Whitesides, G. M. Elastomeric Origami: Programmable Paper-Elastomer Composites as Pneumatic Actuators. *Adv. Funct. Mater.* **2012,** *22* (7), 1376-1384.

(15) Guvendiren, M.; Burdick, J. A.; Yang, S. Solvent Induced Transition from Wrinkles to Creases in Thin Film Gels with Depth-Wise Crosslinking Gradients. *Soft Matter* **2010,** *6* (22), 5795-5801.

(16) Xu, B.; Hayward, R. C. Low-Voltage Switching of Crease Patterns on Hydrogel Surfaces. *Adv. Mater.* **2013,** *25* (39), 5555-5559.

(17) Xu, B. B.; Liu, Q.; Suo, Z.; Hayward, R. C. Reversible Electrochemically Triggered Delamination Blistering of Hydrogel Films on Micropatterned Electrodes. *Adv. Funct. Mater.* **2016,** *26* (19), 3218-3225.

(18) Yang, C.; Suo, Z. Hydrogel Ionotronics. *Nat. Rev. Mater.* **2018,** *3* (6), 125-142.

(19) Liu, K.; Zhang, Y.; Cao, H.; Liu, H.; Geng, Y.; Yuan, W.; Zhou, J.; Wu, Z. L.; Shan, G.; Bao, Y.; Zhao, Q.; Xie, T.; Pan, P. Programmable Reversible Shape Transformation of Hydrogels Based on Transient Structural Anisotropy. *Adv. Mater.* **2020,** *32* (28), 2001693.

(20) Yuk, H.; Lin, S.; Ma, C.; Takaffoli, M.; Fang, N. X.; Zhao, X. Hydraulic Hydrogel Actuators and Robots Optically and Sonically Camouflaged in Water. *Nat. Commun.* **2017,** *8*, 14230.

(21) Li, M.; Wang, X.; Dong, B.; Sitti, M. In-Air Fast Response and High Speed Jumping and Rolling of a Light-Driven Hydrogel Actuator. *Nat. Commun.* **2020,** *11* (1), 3988.

(22) Ionov, L. Hydrogel-Based Actuators: Possibilities and Limitations. *Mater. Today* **2014,** *17* (10), 494-503.

(23) Kim, C.-C.; Lee, H.-H.; Oh, K. H.; Sun, J.-Y. Highly Stretchable, Transparent Ionic Touch Panel. *Science* **2016,** *353* (6300), 682-687.

(24) Liu, X.; Liu, J.; Lin, S.; Zhao, X. Hydrogel Machines. *Mater. Today* **2020,** *36*, 102-124.

(25) Palleau, E.; Morales, D.; Dickey, M. D.; Velev, O. D. Reversible Patterning and Actuation of Hydrogels by Electrically Assisted Ionoprinting. *Nat. Commun.* **2013,** *4*, 2257.

(26) Xu, B.; Han, X.; Hu, Y.; Luo, Y.; Chen, C. H.; Chen, Z.; Shi, P. A Remotely Controlled Transformable Soft Robot Based on Engineered Cardiac Tissue Construct. *Small* **2019,** *15* (18), 1900006.

(27) Li, F.; Hou, H.; Yin, J.; Jiang, X. Near-Infrared Light-Responsive Dynamic Wrinkle Patterns. *Sci. Adv.* **2018,** *4* (4), eaar5762.

(28) Wang, T.; Yang, Y.; Fu, C.; Liu, F.; Wang, K.; Xu, F. Wrinkling and Smoothing of a Soft Shell. *J. Mech. Phys. Solids* **2020,** *134*, 103738.

(29) Ma, T.; Li, T.; Zhou, L.; Ma, X.; Yin, J.; Jiang, X. Dynamic Wrinkling Pattern Exhibiting Tunable Fluorescence for Anticounterfeiting Applications. *Nat. Commun.* **2020,** *11* (1), 1811.

(30) Yang, S.; Khare, K.; Lin, P.-C. Harnessing Surface Wrinkle Patterns in Soft Matter. *Adv. Funct. Mater.* **2010,** *20* (16), 2550-2564.

(31) Stoop, N.; Lagrange, R.; Terwagne, D.; Reis, P. M.; Dunkel, J. Curvature-Induced Symmetry Breaking Determines Elastic Surface Patterns. *Nat. Mater.* **2015,** *14* (3), 337-342.

(32) Li, T.; Hu, K.; Ma, X.; Zhang, W.; Yin, J.; Jiang, X. Hierarchical 3D Patterns with Dynamic Wrinkles Produced by a Photocontrolled Diels-Alder Reaction on the Surface. *Adv. Mater.* **2020,** *32* (7), 1906712.

(33) Liu, L.; Onck, P. R. Topographical Changes in Photo-Responsive Liquid Crystal Films: A Computational Analysis. *Soft Matter* **2018,** *14* (12), 2411-2428.

(34) Liu, Q.; Ouchi, T.; Jin, L.; Hayward, R.; Suo, Z. Elastocapillary Crease. *Phys. Rev. Lett.* **2019,** *122* (9), 098003.

(35) Trujillo, V.; Kim, J.; Hayward, R. C. Creasing Instability of Surface-Attached Hydrogels. *Soft Matter* **2008,** *4* (3), 564-569.

(36) Jin, L.; Cai, S.; Suo, Z. Creases in Soft Tissues Generated by Growth. *Europhys. Lett.* **2011,** *95* (6), 64002.

(37) Kim, J.; Yoon, J.; Hayward, R. C. Dynamic Display of Biomolecular Patterns through an Elastic Creasing Instability of Stimuli-Responsive Hydrogels. *Nat. Mater.* **2010,** *9* (2), 159-164.

(38) Kim, P.; Abkarian, M.; Stone, H. A. Hierarchical Folding of Elastic Membranes under Biaxial Compressive Stress. *Nat. Commun.* **2011,** *10* (12), 952-957.

(39) Al-Rashed, R.; Jimenez, F. L.; Marthelot, J.; Reis, P. M. Buckling Patterns in Biaxially Pre-Stretched Bilayer Shells: Wrinkles, Creases, Folds and Fracture-Like Ridges. *Soft Matter* **2017,** *13* (43), 7969-7978.

(40) Ebata, Y.; Croll, A. B.; Crosby, A. J. Wrinkling and Strain Localizations in Polymer Thin Films. *Soft Matter* **2012,** *8* (35), 9086-9091.

(41) Yang, Y.; Dai, H. H.; Xu, F.; Potier-Ferry, M. Pattern Transitions in a Soft Cylindrical Shell. *Phys. Rev. Lett.* **2018,** *120* (21), 215503.

(42) Ouchi, T.; Yang, J.; Suo, Z.; Hayward, R. C. Effects of Stiff Film Pattern Geometry on Surface Buckling Instabilities of Elastic Bilayers. *ACS Appl. Mater. Inter.* **2018,** *10* (27), 23406-23413.

(43) Jin, L. Mechanical Instabilities of Soft Materials: Creases, Wrinkles, Folds, and Ridges. Doctoral Dissertation, Harvard University, 2014.

(44) Edmondson, S.; Frieda, K.; Comrie, J. E.; Onck, P. R.; Huck, W. T. S. Buckling in Quasi-2D

Polymers. *Adv. Mater.* **2006,** *18* (6), 724-728.

(45) Nojoomi, A.; Arslan, H.; Lee, K.; Yum, K. Bioinspired 3D Structures with Programmable Morphologies and Motions. *Nat. Commun.* **2018,** *9* (1), 3705.

(46) Zhao, Q.; Yang, X. X.; Ma, C. X.; Chen, D.; Bai, H.; Li, T. F.; Yang, W.; Xie, T. A Bioinspired Reversible Snapping Hydrogel Assembly. *Mater. Horiz.* **2016,** *3* (5), 422-428.

(47) Holmes, D. P.; Roché, M.; Sinha, T.; Stone, H. A. Bending and Twisting of Soft Materials by Non-Homogenous Swelling. *Soft Matter* **2011,** *7* (11), 5188-5193.

(48) Na, J. H.; Evans, A. A.; Bae, J.; Chiappelli, M. C.; Santangelo, C. D.; Lang, R. J.; Hull, T. C.; Hayward, R. C. Programming Reversibly Self-Folding Origami with Micropatterned Photo-Crosslinkable Polymer Trilayers. *Adv. Mater.* **2015,** *27* (1), 79-85.

(49) Angelo, C.; Yoon, C.; Liu, J.; Huang, Q.; Guo, J.; Nguyen, T. D.; Gracias, D. H.; Schulman, R. DNA Sequence−Directed Shape Change of Photopatterned Hydrogels via High-Degree Swelling. *Science* **2017,** *357*, 1126-1130.

(50) Wang, Z. J.; Hong, W.; Wu, Z. L.; Zheng, Q. Site-Specific Pre-Swelling-Directed Morphing Structures of Patterned Hydrogels. *Angew. Chem. Int. Ed.* **2017,** *56* (50), 15974-15978.

(51) Fan, W.; Shan, C.; Guo, H.; Sang, J.; Wang, R.; Zheng, R.; Sui, K.; Nie, Z. Dual-Gradient Enabled Ultrafast Biomimetic Snapping Hydrogel Materials of Hydrogel Materials. *Sci. Adv.* **2019,** *5*, eaav7174.

(52) Zhou, Y.; Duque, C. M.; Santangelo, C. D.; Hayward, R. C. Biasing Buckling Direction in Shape-Programmable Hydrogel Sheets with through-Thickness Gradients. *Adv. Funct. Mater.*

2019, *29* (48), 1905273.

(53) Lee, H.; Zhang, J.; Jiang, H.; Fang, N. X. Prescribed Pattern Transformation in Swelling Gel Tubes by Elastic Instability. *Phys. Rev. Lett.* **2012,** *108* (21), 214304.

(54) Arifuzzaman, M.; Wu, Z. L.; Takahashi, R.; Kurokawa, T.; Nakajima, T.; Gong, J. P. Geometric and Edge Effects on Swelling-Induced Ordered Structure Formation in Polyelectrolyte Hydrogels. *Macromolecules* **2013,** *46* (22), 9083-9090.

(55) Takahashi, R.; Ikura, Y.; King, D. R.; Nonoyama, T.; Nakajima, T.; Kurokawa, T.; Kuroda, H.; Tonegawa, Y.; Gong, J. P. Coupled Instabilities of Surface Crease and Bulk Bending during Fast Free Swelling of Hydrogels. *Soft Matter* **2016,** *12* (23), 5081-5088.

(56) Pezzulla, M.; Stoop, N.; Steranka, M. P.; Bade, A. J.; Holmes, D. P. Curvature-Induced Instabilities of Shells. *Phys. Rev. Lett.* **2018,** *120* (4), 048002.

(57) Pezzulla, M.; Stoop, N.; Jiang, X.; Holmes, D. P. Curvature-Driven Morphing of Non-Euclidean Shells. *Proc. Roy. Soc. A-Math. Phy.* **2017,** *473* (2201), 20170087.

(58) Stein-Montalvo, L.; Costa, P.; Pezzulla, M.; Holmes, D. P. Buckling of Geometrically Confined Shells. *Soft Matter* **2019,** *15* (6), 1215-1222.

(59) Tanaka, T.; Sun, S.; Hirokawa, Y.; Katayama, S.; Kucera, J.; Hirose, Y.; Amiya, T. Mechanical Instability of Gels at the Phase Transition. *Nature* **1987,** *325* (26), 796-798.

(60) Tanaka, T.; Sun, S. T.; Hirokawa, Y.; Katayama, S.; Kucera, J.; Hirose, Y.; Amiya, T. *Mechanical Instability of Swelling Gels*, Studies in Polymer Science ed.; Elsevier Science Publishers B.V.: Amsterdam, 1988.

(61) Takahashi, K.; Takigawa, T.; Masuda, T. Swelling and Deswelling Kinetics of Poly(N-Isopropylacrylamide) Gels. *J. Chem. Phys.* **2004,** *120* (6), 2972-2979.

(62) Li, Y.; Tanaka, T. Kinetics of Swelling and Shrinking of Gels. *J. Chem. Phys.* **1990,** *92* (2), 1365-1371.

Table of Contents Graphic

The autonomous shape morphing with good reproducibility of ‘semi-cylinder shell’ hydrogel from ‘open’ to ‘close’ to ‘reopen’ were induced by instabilities of buckling and creasing during free swelling.